Master Thesis

Nutrient Driven Topology Optimization

Ganarupan Satha

Linköping 2010

LIU-IEI-TEK-A-10/00865-SE

INSTITUTE OF TECHNOLOGY
LINKÖPING UNIVERSITY

Division of Mechanics
Department of Management and Engineering (IEI)
Linköpings universitet, SE-581 83 Linköping, Sweden

Nutrient Driven Topology Optimization

Master's thesis project conducted at
Division of Mechanics
Linköpings universitet
by

Ganarupan Satha

LIU-IEI-TEK-A-10/00865-SE

Supervisor and Examiner: **Anders Klarbring**
IEI, Linköpings Universitet

Linköping, 14 June, 2010

Abstract

The aim of this thesis is to investigate how a biological structure changes its shape and boundary under different cases of load if flow of nutrients is included, since nutrient flow has not been taken into account in previous studies.

In order to simulate such a scenario we construct a model by using topology optimization (the SIMP model) and a balance law which is suitable for biological structures. Moreover, the model is derived by using an analogy with the dissipation inequality and Coleman-Noll's procedure. The model can be interpreted as bone or some other biological structure, where the growth and remodeling partly occurs due to nutrient flow.

The theory is first investigated by selecting an MBB beam with a special boundary condition for the nutrient concentration and inflow of nutrients, and then with a bone-like model.

For the analysis with different loads we have observed that the structure becomes thicker were the load is applied. Parameters like beta (β) (reflecting the relation between nutrients and material) and nutrient concentration (c) seem to play an important role in nutrient transport and building of the structure. The result for larger values of β and nutrient concentration (c) gives a thicker structure in the entire domain. We also made an assumption of Fick's law of diffusion. Fick's law of diffusion describes the flux from high concentration to low concentration. This phenomenon is observed in analysis with different nutrient concentrations (c): we can see that the structure tends to be built up where the concentration is high and continues to be built in the direction from high to low concentration. In analyses with mu-value (μ), which represents cost of material, the result gives a thinner structure for larger values of μ.

Acknowledgements

This master thesis is the final project in the programme for a Master of Science degree in Mechanical Engineering. The work has been carried out at the Division of Mechanics of the Institute of Technology at Linköping University in a research project for Professor Anders Klarbring.

I would like to thank my supervisor Anders Klarbring for always being available for discussion on the theoretical background, for help in choosing a model to investigate and tips regarding the master thesis report.

Also I would like to thank my co-supervisor Bo Torstenfelt at Division of Solid Mechanics, Linköping University, for always being available for discussion about FEM models and help in programming.

I also thank all staff at the Division of Mechanics for their help and support.

Finally, I would also like to thank my family and friends for their support.

Contents

List of Figures

List of Tables

Chapter 1

Introduction

All biological structures need to be optimized to function well in their respective contexts, including carrying out specific functions (such as transport, respiration or structural support) and at the same time allowing for their own maintenance and inflow of nutrients. A challenge in medical engineering is to design implants that have the above qualities, for example, bone implants need to be structurally optimized to be able to carry a certain load [1]. The load carried by bone depends on the shape of the bone implant, which distributes the load to the bone. There are many factors affecting bone implant failure, for instance, diseases and damage. Another factor can be that the load carried by bone through the bone implant is not uniformly distributed. That implies that the bone disappears where the load is low.

In a recent study [2], Klarbring and Torstenfelt studied a dynamical systems approach to investigate the material distribution by a topology optimization formulation. They found a connection between optimization problems and natural evolution such as bone remodeling and damage evolution. In addition, they investigated different types of algorithms. Moreover in [3],[4], [5] Harrigan and Hamilton investigated the stability and uniqueness of the solution to a bone remodeling simulation. In these studies the nutrient influence is not taken in account.

The purpose of this project is to investigate how a structure changes its shape and boundary, if flow of nutrients is included. In order to simulate this kind of property we construct a model by using topology optimization (the SIMP model) and a balance law which is suitable for biological structures. Moreover, the model is derived by using an analogy with the dissipation inequality and Coleman-Noll's procedure. The model can be interpreted as bone or some other biological structure, where the growth and remodeling occurs due to nutrient flow.

This thesis comprises several chapters: In the second chapter a general background is given where the theory is described and a balance law suitable for biological structures is derived. In the third chapter, a model with inflow of nutrients is derived. The fourth chapter explains implementation in TRINITAS for a steady state model which means that all time derivative is zero. In the fifth chapter a problem is selected with special boundary conditions for the nutrients. In chapter

six the results for the selected problem is presented. The seventh chapter contains discussion about the results, the equations and about the selected problems etc.

To understand the thesis one should have some basic background about structural optimization, finite element analysis, models of mechanics and some knowledge about biological processes.

Chapter 2

Background

In this chapter we describe the dynamical system, the SIMP model and the dissipation inequality. In addition, we also derive a balance law, which is suitable for a biological structure with growth, remodeling and inflow of nutrients. Let us start by discussing a biological structure such as a bone, in order to get an insight into what a biological structure is.

2.1 Bone

The adult skeletal system of the human body consists of 206 bones and the various structures forming the joints between them. The skeleton provides mechanical support and protection for the organs. In the skeletal system we can find five different kinds of bones based on shape. These are long, short, flat, irregular and sesamoid bones. Long bones include bones of the thighs, legs, toes and arms. Short bones include the wrist and ankle bones. Flat bones include the cranial bones, sternum (breastbone), ribs and scapulas (shoulder blades). The irregular bones have complex shapes. The sesamoid bones are small bones. Bone is a kind of structure that always changes shape, mass and material properties depending on age, diseases and physical activities of the individual. According to Wolff's law the bone grows and remodels in response to applied load. Let us look at the structure, composition and cells of the bone [6].

2.1.1 Structure of bone

Bone is not simply a solid but in fact a living tissue, and all bone has some spaces between the solid parts. The space makes it easier to provide channels for blood vessels that supply bone cells with nutrients. To examine the structure of the bone we can divide the structure into macroscopic and microscopic levels. Let us start with the macroscopic level.

At the macroscopic level bone occurs in two forms; compact (cortical) bone and cancellous (trabecular) bone (figure 2.1 shows the structure and parts of a long bone). Compact bone is a dense material due to its minimal gaps and spaces.

Nearly 80 procent of the skeletal mass in the adult human skeleton is compact bone. Compact bone constitutes the wall of all bones and is responsible for the supportive and protective function of the skeleton. The compact bone is made up of a structure of haversian systems or osteons with lamellae in concentric circles with collagen fibrils. In the centre of each haversian systems is a canal which is lined by endosteum containing blood vessels. The remaining 20 procent of skeleton is cancellous bone, which is found in the inner parts of bones. The fraction of the skeletal mass made up by compact bone, compared to the fraction made up by cancellous bone, varies from person to person.

At the microscopic level the cancellous bone is of two types, woven or lamellar. In woven bone, collagen fibrils are oriented randomly (collagen is a type of protein). In lamellar bone, the collagen fibrils are arranged parallell to each other in a plane. The bone tissues are constantly developing and the structure is optimized; woven bone is found in young children, whereas lamellar bone is found mainly in adults [7], [8].

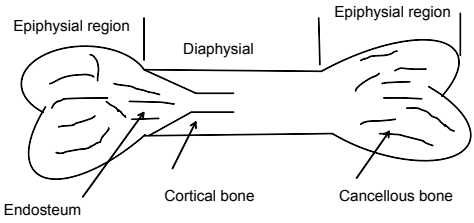

Figure 2.1. The structure and parts of a long bone

2.1.2 Composition of bone

Bone is composed of the mineral hydroxiapatite $Ca_{10}(PO_4)_6(OH)_2$, the fibrous protein collagen, organic matrix, cells and water. Bone therefore serves as a reserve of minerals, especially calcium and phosphorus. Hydroxiapatite and collagen fibrils is responsible for the strength and hardness of bones [7], [8].

2.1.3 The cells of bone

There are several types of bone cells, but three different types of cells, osteoblasts, osteoclasts and osteocytes, are the most important from a mechanical point of view.

Osteoblasts are bone creating cells. Osteoblasts start to form the collagen and other compounds needed to build the bone. Osteoblasts regulate the flow of calcium and phosphate into and out of bone. They are also active in the calcification and resorption of bone.

Osteoclasts are bone destroying cells and maintain daily celluar activites within the bone, which is important in development, growth, maintance and repair of bone.

Osteocytes are resident bone cells. The osteocytes appear after new bone has been formed. They are believed to function as mechanical sensors in the bone and send chemical signals to activate the osteoclasts and osteoblasts to maintain the bone remodeling and growth [7], [8].

2.2 Topology optimization

By using topology optimization many applications have been solved [9]. Topology optimization as a material distribution problem has changed the design process in many industries in the last decades, for instance in the automotive industry and in bioscience. Topology optimization is used at an initial design stage to get a suitable solution. Nowadays the field of computer science has grown fast and combined with more computing power it is possible to perform more advanced calculations. The benefits from topology optimization as a material distribution problem is that it gives design proposals with new shapes under a given constraint and boundary conditions. The design problem gives a 0-1 distribution of material, which means that we get a design with holes and material, respectively.

2.2.1 The SIMP model

In classical topology and sizing optimization we minimize the compliance in order to get a stiff structure under a given constraint and boundary conditions. By using the SIMP (Solid Isotropic Materials with Penalization) model we get a design with holes and material. In order to explain the SIMP model we state a classical structural optimization problem as minimizing the objective function $g_C(\boldsymbol{\rho})$.

$$\min_{\boldsymbol{\rho}} \; g_C(\boldsymbol{\rho}) = \frac{1}{2}\mathbf{F}^T\mathbf{u}(\boldsymbol{\rho})$$

s.t

$$\sum_{i=1}^{E} a_i\rho_i \leq V$$

$$0 \leq \rho \leq 1$$

where

- V is total the volume of the domain
- $\mathbf{F}$ is a force vector

- $\mathbf{u}$ is a displacement vector
- a_i are element areas
- $\boldsymbol{\rho} = (\rho_i)$ is a design variable

In this problem we are seeking a stiff structure by using a volume or mass constraint with design variable $\boldsymbol{\rho}$. The quasi-static equilibrium equation for a linear discrete structure is stated below:

$$\mathbf{F} = \mathbf{K}(\boldsymbol{\rho})\mathbf{u} \tag{2.1}$$

Here $\mathbf{K}(\boldsymbol{\rho})$ is the stiffness matrix and it depends on the design variable $\boldsymbol{\rho}$. The stiffness matrix is symmetric and positive semi definite. In order to avoid singularity of the stiffness matrix we let the lower bound of $\boldsymbol{\rho}$ be a small fixed value ($\epsilon > 0$). To get a design with holes and material we let the stiffness matrix be as follows:

$$\mathbf{K}(\boldsymbol{\rho}) = \sum_{i=1}^{E} \rho_i^q \tilde{\mathbf{K}}_i$$

Here E is the number of elements and $\tilde{\mathbf{K}}$ is an element stiffness matrix. Letting the penalty parameter $q > 1$ (in topology optimization we let $q = 3$) we get a solution where ρ_i approaches 0 and 1. It is very important to note that if $q = 1$ we get sizing optimization (variable thickness problem), which means that the ρ_i varies linearly between 0 and 1.

By adding a total volume term in the objective function $g_C(\boldsymbol{\rho})$ and removing the volume constraint we get a new optimization problem as a dynamical system and using design variables $\boldsymbol{\rho}$. The objective function becomes as below:

$$f_C(\boldsymbol{\rho}) = \frac{1}{2}\mathbf{F}^T\mathbf{u}(\boldsymbol{\rho}) + \mu \sum_{i=1}^{E} a_i\rho_i$$

Here μ is cost of material. The reason to use the objective function $f_C(\boldsymbol{\rho})$ is that it plays an important role in bone remodeling, see [2], [3], [4], [5] and [10]. Having a volume constraint for biological structures is not relevant, as they grow freely with respect to volume.

2.3 Dynamical systems

In this section we are going to study a dynamical systems approach in order to use it to investigate the material distribution problem. Assume that we study a dynamical system such as

$$\frac{dx(t)}{dt} = -\nabla f(x(t))$$

where t is a time-like variable and $x(t)$ is the solution trajectory. The dynamical system has an equilibrium point x_0 defined by $\nabla f(x_0) = 0$. Let us have a function $f(x)$ with the properties

$$f(x_0) = 0;\ f(x(t)) > 0,\ x(t) \neq x_0;$$

$$\frac{d}{dt}f(x(t)) = \nabla f(x(t))\dot{x}(t) = -\nabla f(x(t))\nabla f(x(t)) \leq 0$$

If these properties hold for the function f in the surroundings of the equilibrium point x_0, it is said to be a Lyaponov function and the function decreases along the trajectory. The function f can be an energy function, where we can find the value of the variable x that minimizes the energy function [10].

2.4 Dissipation inequality

Thermodynamics is the science of energy. Energy can be found in various forms, for instance mechanical work, mass transport and heat transfer. Energy cannot be created or destroyed, but only changed into another form. These energy changes are described by the first and second laws of thermodynamics.

The first law of thermodynamics states that the change of internal energy of a system is equal to the sum of heat energy, inflow of energy and work performed on the system.

$$\dot{U} = Q + M + W \tag{2.2}$$

where

- $\dot{(\,)}$ is a time derivative
- U is the internal energy
- W is the work per unit time
- M is the inflow of energy by mass transport (in our case we have nutrients (blood, water etc)) per unit time
- Q is the heat supply per unit time

The second law of thermodynamics states that

$$\dot{s} \geq \frac{Q}{T} \tag{2.3}$$

Here s is the entropy and T is the absolute temperature. The equality holds for reversible processes and the inequality for irreversible ones. Here we make an assumption of an isothermal process, which means that the temperature is constant in the system.

The free energy can be written as

$$\psi = U - sT \tag{2.4}$$

Taking the time derivative of equation (2.4), we obtain

$$\dot{\psi} = \dot{U} - \dot{s}T \tag{2.5}$$

From equation (2.2), (2.5) and inequality (2.3), we then get a dissipation inequality as

$$\dot{\psi} \leq M + W \tag{2.6}$$

According to the dissipation inequality, the rate of free energy cannot be larger than the sum of work and inflow of energy.

Once the dissipation inequality is derived from the first and second laws of thermodynamics, we can use it to derive a dynamical system. Let us formulate the dissipation inequality in the following way in order to show this fact:

$$\psi = \frac{1}{2}\mathbf{u}^T\mathbf{K}(\boldsymbol{\rho})\mathbf{u} \tag{2.7}$$

$$W = \mathbf{F}^T\dot{\mathbf{u}} \tag{2.8}$$

$$M = \mathbf{r}^T\dot{\boldsymbol{\rho}} \tag{2.9}$$

The equation (2.7) is the strain energy for a discrete structure and it is non-negative, since the stiffness matrix is positive semidefinite. Equation (2.8) is the work per unit time. The relation (2.9) decribes the biological remodeling or growth, where $\mathbf{r}$ can be seen as remodeling force. Taking the time derivative of equation (2.7), we obtain

$$\dot{\psi} = \sum_{i=1}^{E}\frac{1}{2}\mathbf{u}^T\frac{\partial\mathbf{K}}{\partial\rho_i}\mathbf{u}\dot{\rho}_i + \mathbf{u}^T\mathbf{K}(\boldsymbol{\rho})\dot{\mathbf{u}} \tag{2.10}$$

Using equations (2.8), (2.9), (2.10) and the inequality (2.6), we obtain

$$\sum_{i=1}^{E}\left(\frac{1}{2}\mathbf{u}^T\frac{\partial\mathbf{K}}{\partial\rho_i}\mathbf{u} - r_i\right)\dot{\rho}_i + \left(\mathbf{u}^T\mathbf{K}(\boldsymbol{\rho}) - \mathbf{F}^T\right)\dot{\mathbf{u}} \leq 0 \tag{2.11}$$

Since we have a relation (2.1), that reduces the inequality as below:

$$\sum_{i=1}^{E}\left(\frac{1}{2}\mathbf{u}^T\frac{\partial\mathbf{K}}{\partial\rho_i}\mathbf{u} - r_i\right)\dot{\rho}_i \leq 0 \tag{2.12}$$

The inequality above is satisfied if

$$-\tilde{k}_i\dot{\rho}_i \in \frac{1}{2}\mathbf{u}^T\frac{\partial\mathbf{K}}{\partial\rho_i}\mathbf{u} - r_i + \partial I_{K_i}(\rho_i) \tag{2.13}$$

where $\tilde{k}_i$ is a positive function of $\boldsymbol{\rho}$ and its time derivative. The $\partial I_{K_i}(\rho_i)$ is a subdifferential (see Appendix) of an indicator function of the set $K_i = \{\rho_i | \epsilon \leq \rho_i \leq 1\}$. Deriving the relation (2.1) and (2.13) in this way is called Coleman-Noll's procedure [11].

Let us prove that the relation (2.13) satisfies the inequality (2.12). The relation (2.13) becomes as below

$$-\tilde{k}_i\dot{\rho}_i = \frac{1}{2}\mathbf{u}^T\frac{\partial\mathbf{K}}{\partial\rho_i}\mathbf{u} - r_i + \bar{\lambda}_i + \underline{\lambda}_i \tag{2.14}$$

$$\bar{\lambda}_i(\rho_i - 1) = 0 \quad \bar{\lambda}_i \geq 0 \quad , \rho_i \leq 1 \tag{2.15}$$

$$\underline{\lambda}_i(\epsilon - \rho_i) = 0 \quad \underline{\lambda}_i \geq 0 \quad , \epsilon \leq \rho_i \tag{2.16}$$

Here we use the Karush-Kuhn-Tucker (KKT) condition. Taking the time derivative of equation (2.15) and (2.16) gives

$$\dot{\bar{\lambda}}_i(\rho_i - 1) + \bar{\lambda}_i\dot{\rho}_i = 0 \tag{2.17}$$

$$\dot{\underline{\lambda}}_i(\epsilon - \rho_i) + \underline{\lambda}_i\dot{\rho}_i = 0 \tag{2.18}$$

For the equation (2.17) we have two cases. In the first case, $\dot{\bar{\lambda}}_i = 0$ and $\rho_i - 1 \neq 0$. In the second case, $\dot{\bar{\lambda}}_i \neq 0$ and $\rho_i - 1 = 0$. The same principle applies to (2.18). That gives

$$\bar{\lambda}_i\dot{\rho}_i = 0 \tag{2.19}$$

$$\underline{\lambda}_i\dot{\rho}_i = 0 \tag{2.20}$$

By using equations (2.14), (2.19) and (2.20) into (2.12), we obtain

$$-\sum_{i=1}^{E} \tilde{k}_i\dot{\rho}_i^2 \leq 0 \tag{2.21}$$

Here we note that the term $\sum_{i=1}^{E} \tilde{k}_i\dot{\rho}_i^2$ is positive and the inequality (2.12) is satisfied [10], [12].

2.5 Balance law

All living organisms need nutrients to stay alive. Nutrients are chemical substances in food that provide energy, form new body components, or assist in the functioning of various body processes. The classes of nutrients are carbonhydrates, proteins, fat, minerals, vitamins and water [13].

Let us think about bone as a living organism that needs nutrients to maintain the optimal structure and repair damaged structure. Bone contains very complex vascular structures that transport nutrients. We can think about a model of bone as the figure 2.2, that represents a part $\Omega^{'}$ of the domain Ω.

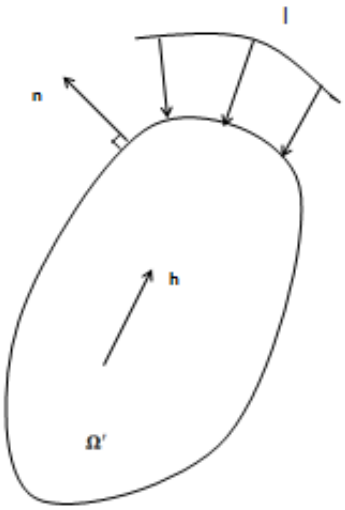

Figure 2.2. A part $\Omega^{'}$ of the domain Ω

Let us formulate the balance law for the domain $\Omega^{'}$.

$$\int_{\Omega'} \dot{c}\, d\Omega^{'} = -\int_{\delta\Omega'} \mathbf{h}\cdot\mathbf{n}\, dA + \int_{\Omega'} (m - \beta\dot{\rho})\, d\Omega^{'} \tag{2.22}$$

where

- c is the nutrient concentration
- $\mathbf{h}$ is the nutrient flow vector
- m is the body inflow of nutrients
- β is the relation between nutrients and material
- $\mathbf{n}$ is normal unit vector that is directed outwards

By using Gauss divergence theorem, see [14], in equation (2.22) we get

$$\int_{\Omega'} \dot{c}\, d\Omega' = -\int_{\Omega'} \mathrm{div}\mathbf{h}\, d\Omega' + \int_{\Omega'} (m - \beta\dot{\rho})\, d\Omega'$$

which implies

$$\int_{\Omega'} (\dot{c} + \mathrm{div}\mathbf{h} - m + \beta\dot{\rho})\, d\Omega' = 0$$

By using the localization theorem, see [15], we get

$$\dot{c} + \mathrm{div}\mathbf{h} = m - \beta\dot{\rho} \quad \text{in } \Omega \tag{2.23}$$

On the boundary $\partial\Omega$, we let

$$\mathbf{h} \cdot \mathbf{n} = l \tag{2.24}$$

where l is a magnitude of nutrient flow in $\mathbf{n}$ direction.

2.5.1 Discrete form of the balance law

The balance law above is in continuum form, but in order to perform finite element calculations we have to write the balance law in discrete form. The first step to achieve the discrete form is to multiply (2.23) by an arbitrary weight function w and integrate over the domain Ω:

$$\int_{\Omega} (\dot{c} + \mathrm{div}\mathbf{h} - m + \beta\dot{\rho})\, w\, d\Omega = 0 \tag{2.25}$$

The equation above can be developed in the following way:

$$\int_{\Omega} (\dot{c} - m + \beta\dot{\rho})\, w\, d\Omega + \int_{\Omega} \mathrm{div}\mathbf{h} w\, d\Omega = 0 \tag{2.26}$$

and using the formula $\mathrm{div}(w\mathbf{h}) = w\mathrm{div}\mathbf{h} + \mathbf{h} \cdot \nabla w$ in equation (2.26) we get

$$\int_{\Omega} (\dot{c} - m + \beta\dot{\rho})\, w\, d\Omega + \int_{\Omega} (-\mathbf{h} \cdot \nabla w + \mathrm{div}(w\mathbf{h}))\, d\Omega = 0 \tag{2.27}$$

Now by using the Gauss divergence theorem and equation (2.24) in equation (2.27) we get

$$\int_{\Omega} (\dot{c} - m + \beta\dot{\rho})\, w\, d\Omega + \int_{\Omega} (-\mathbf{h} \cdot \nabla w)\, d\Omega + \int_{\partial\Omega} wl\, dA = 0 \tag{2.28}$$

Equation (2.28) is the weak form of (2.23) and (2.24). The second step to achieve the discrete form is letting the weight function have a form like below:

$$w(x) = \mathbf{v}^T \mathbf{N}(x)^T \tag{2.29}$$

$$\nabla w(x) = \mathbf{v}^T \mathbf{B}(x)^T \tag{2.30}$$

Where $\mathbf{N}$ is the shape function, $\mathbf{v}$ is the nodal virtual nutrient concentration and $\mathbf{B}$ is the derivate of the shape function. Inserting (2.29) and (2.30) into (2.28), gives

$$\mathbf{v}^T \left(\int_\Omega \left(\dot{c} - m + \beta \dot{\rho} \right) \mathbf{N}^T d\Omega + \int_\Omega \left(-\mathbf{h}\mathbf{B}^T \right) d\Omega + \int_{\partial\Omega} \mathbf{N}^T l dA \right) = 0 \quad \forall \ \mathbf{v}^T \tag{2.31}$$

This implies

$$\int_\Omega \dot{c}\mathbf{N}^T d\Omega - \int_\Omega \mathbf{h}\mathbf{B}^T d\Omega = \int_\Omega m\mathbf{N}^T d\Omega - \int_\Omega \beta\dot{\rho}\mathbf{N}^T d\Omega - \int_{\partial\Omega} \mathbf{N}^T l dA \tag{2.32}$$

Equation (2.32) can be written in a simpler way. Here we define

$$\dot{\mathbf{c}} = \int_\Omega \dot{c}\mathbf{N}^T d\Omega$$

$$\mathbf{m} = \int_\Omega m\mathbf{N}^T d\Omega - \int_{\partial\Omega} \mathbf{N}^T l dA$$

$$\widetilde{\mathbf{N}}\mathbf{a} = \int_\Omega \mathbf{N}^T d\Omega \tag{2.33}$$

$$\widetilde{\mathbf{B}}^T \tilde{\mathbf{h}} = -\int_\Omega \mathbf{h}\mathbf{B}^T d\Omega \tag{2.34}$$

Let us explain the relation (2.34) by using a numerical integration method (see [16], [17] and [18]). In FE programs, Gauss integration method is used especially for isoparametric elements. In this thesis we are going to use mostly a four-node isoparametric element. This element has 2x2 Gauss integration points (see figure 2.3), two Gauss points in the η- direction and two in ξ-direction. Equation (2.34) is explained as follows:

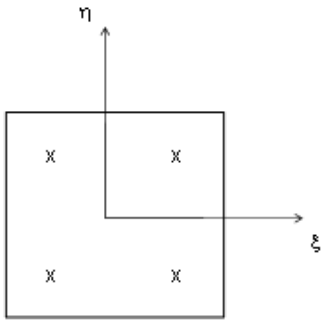

Figure 2.3. Locations of Gauss points for the four-node isoparametric element

$$-\int_{\Omega} \mathbf{h}\mathbf{B}^T d\Omega = \sum_{i=1}^{E}\sum_{k=1}^{4} \mathbf{h}^T(x_k)\mathbf{B}(x_k) = \sum_{i=1}^{E} \bar{\mathbf{h}}^T\bar{\mathbf{B}} = \widetilde{\mathbf{B}}^T\tilde{\mathbf{h}}$$

In the first step we calculate values for each Gauss point according to figure 2.3 and sum up all four values for each element. The dimension for $\mathbf{h}^T$ is 1×2 and for $\mathbf{B}$ is $2 \times N$. In the second step we sum the calculated result for all elements, the dimension for $\bar{\mathbf{h}}^T$ is $1 \times 2 \cdot 4$ and for $\bar{\mathbf{B}}$ is $4 \cdot 2 \times N$. Concerning the relation 2.33, in FE program we use mapping from the reference element (four-node isoparametric element) to the global domain. In the mapping we transform the reference element to another coordinate system and in this transformation an area or volume change occurs, that is noted in 2.33.

Now we can write equation (2.32) in the following way

$$\dot{\mathbf{c}} + \widetilde{\mathbf{B}}^T\tilde{\mathbf{h}} = \mathbf{m} - \beta\widetilde{\mathbf{N}}\dot{\rho}\mathbf{a}$$

Where $\mathbf{m}$ is the nodal inflow of nutrients and $\mathbf{c}$ is the nodal values of nutrient concentration.

The balance law can now be written for an element;

$$\dot{c}_k + \widetilde{\mathbf{B}}_k^T\tilde{\mathbf{h}} = m_k - \beta\sum_{i=1}^{E} \tilde{N}_{ki}\dot{\rho}_i a_i \tag{2.35}$$

where $\widetilde{\mathbf{B}}_k$ is row of $\widetilde{\mathbf{B}}$ and $\widetilde{N}_{ki}$ is an element of $\widetilde{\mathbf{N}}$.

Chapter 3

Model with inflow of nutrients

In this chapter we construct a model with inflow of nutrients by using the analogy with the dissipation inequality. In left hand side of an inequality we use

$$f_C^e(\boldsymbol{\rho}, \mathbf{c}) = f_C(\boldsymbol{\rho}) + \psi(\mathbf{c}) \tag{3.1}$$

The $f_C(\boldsymbol{\rho})$ is the same function as was defined in the section on topology optimization. By adding a function $\psi(\mathbf{c})$ to $f_C(\boldsymbol{\rho})$ we introduce the nutrients flow in our model. Here $\psi(\mathbf{c})$ is assumed to be a quadratic function defined by a constant γ. The expression for the $\psi(\mathbf{c})$ is

$$\psi(\mathbf{c}) = \frac{1}{2}\gamma c^2$$

By analogy with the dissipation inequality we formulate our right hand side by using the term below. The term describes the inflow of energy into the system:

$$\sum_{k=1}^{N} \tilde{\mu}_k m_k \tag{3.2}$$

where $\tilde{\mu}_k$ is a chemical potential. Taking the time derivative of (3.1) and using the relation for inflow of energy we create an inequality as follows:

$$\frac{d}{dt} f_C^e(\boldsymbol{\rho}, \mathbf{c}) \leq \sum_{k=1}^{N} \tilde{\mu}_k m_k \tag{3.3}$$

By using equation (2.35) and (3.3) we get

$$\sum_{i=1}^{E} \frac{\partial f_C(\boldsymbol{\rho})}{\partial \rho_i} \dot{\rho}_i + \sum_{k=1}^{N} \frac{\partial \psi(\mathbf{c})}{\partial c_k} \dot{c_k} \leq \sum_{k=1}^{N} \tilde{\mu}_k \left(\dot{c}_k + \widetilde{\mathbf{B}}_k^T \tilde{\mathbf{h}} + \beta \sum_{i=1}^{E} \tilde{N}_{ki} \dot{\rho}_i a_i \right) \tag{3.4}$$

This implies

$$\sum_{i=1}^{E}\left(\frac{\partial f_C(\boldsymbol{\rho})}{\partial \rho_i}-\beta\sum_{k=i}^{N}\tilde{\mu}_k\tilde{N}_{ki}a_i\right)\dot{\rho}_i+\sum_{k=1}^{N}\left(\frac{\partial \psi(\mathbf{c})}{\partial c_k}-\tilde{\mu}_k\right)\dot{c_k}-\left(\widetilde{\mathbf{B}}\tilde{\boldsymbol{\mu}}\right)^T\tilde{\mathbf{h}}\leq 0 \quad (3.5)$$

The inequality (3.5) should be valid for all thermodynamic processes. Here we assume that $\tilde{\mu}_k$ only depends on c_k and because of this it is necessary that the inequality implies

$$\tilde{\mu}_k=\frac{\partial \psi(\mathbf{c})}{\partial c_k} \quad (3.6)$$

The second term vanishes and that gives

$$\sum_{i=1}^{E}\left(\frac{\partial f_C(\boldsymbol{\rho})}{\partial \rho_i}-\beta\sum_{k=i}^{N}\tilde{\mu}_k\tilde{N}_{ki}a_i\right)\dot{\rho}_i-\left(\widetilde{\mathbf{B}}\tilde{\boldsymbol{\mu}}\right)^T\tilde{\mathbf{h}}\leq 0 \quad (3.7)$$

The first term of inequality (3.7) can be garantied negative by assuming

$$-\tilde{k}_i\dot{\rho}_i\in\frac{\partial f_C(\boldsymbol{\rho})}{\partial \rho_i}-\beta\sum_{k=i}^{N}\tilde{\mu}_k\tilde{N}_{ki}a_i+\partial I_{K_i}(\rho_i) \quad (3.8)$$

where $\tilde{k}_i$ is a positive function of $\boldsymbol{\rho}$, $\mathbf{c}$ and their time derivatives. The $\partial I_{K_i}(\rho_i)$ is a subdifferential of an indicator function of the set $K_i=\{\rho_i|\epsilon\leq\rho_i\leq 1\}$. The second term of the inequality (3.7) can be made to have the right sign by assuming

$$\tilde{\mathbf{h}}=\mathbf{E}\left(\boldsymbol{\rho}\right)\widetilde{\mathbf{B}}\tilde{\boldsymbol{\mu}} \quad (3.9)$$

When $\mathbf{E}\left(\boldsymbol{\rho}\right)$ is positive definite, This relation is a Fick's law for diffusion of nutrients. Fick's law of diffusion decribes the flux from high concentration to low concentration. In an isotropic case we have

$$\mathbf{E}\left(\boldsymbol{\rho}\right)=\sum_{i=1}^{E}\kappa(\rho_i)\mathbf{I}_i \quad (3.10)$$

where

- $\kappa(\rho_i)$ is the diffusivity
- $\mathbf{I}_i$ are identity-like matrices

The diffusivity $\kappa(\rho_i)$ is assumed to depend linearly on the design:

$$\kappa(\rho_i)=\left(1-\rho_i+\epsilon\right)\kappa_0 \quad (3.11)$$

This relation says that if ρ_i approaches 1 we have a solid material, that means the porosity is close to zero. So the ρ_i is a porosity-like variable and κ_0 is a permeability constant for the bone that can be collected from the litterature. ϵ is a small fixed value.

Let us prove why the relation (3.8) together with (3.9) satisfies the inequality (3.7). Starting with the relation (3.8) it becomes

$$-\tilde{k}_i\dot{\rho}_i = \frac{\partial f_C(\boldsymbol{\rho})}{\partial \rho_i} - \beta \sum_{k=i}^{N} \tilde{\mu}_k \tilde{N}_{ki} a_i + \bar{\lambda}_i + \underline{\lambda}_i \tag{3.12}$$

$$\bar{\lambda}_i(\rho_i - 1) = 0 \quad \bar{\lambda}_i \geq 0 \quad , \rho_i \leq 1 \tag{3.13}$$

$$\underline{\lambda}_i(\epsilon - \rho_i) = 0 \quad \underline{\lambda}_i \geq 0 \quad , \epsilon \leq \rho_i \tag{3.14}$$

Here we use the Karush-Kuhn-Tucker (KKT) conditions. Taking the time derivative of equations (3.13) and (3.14) gives

$$\dot{\bar{\lambda}}_i(\rho_i - 1) + \bar{\lambda}_i\dot{\rho}_i = 0 \tag{3.15}$$

$$\dot{\underline{\lambda}}_i(\epsilon - \rho_i) + \underline{\lambda}_i\dot{\rho}_i = 0 \tag{3.16}$$

For the equation (3.15) we have two cases. In the first case, $\dot{\bar{\lambda}}_i = 0$ and $\rho_i - 1 \neq 0$. In the second case, $\dot{\bar{\lambda}}_i \neq 0$ and $\rho_i - 1 = 0$. The same principle applies to (3.16). That gives

$$\bar{\lambda}_i\dot{\rho}_i = 0 \tag{3.17}$$

$$\underline{\lambda}_i\dot{\rho}_i = 0 \tag{3.18}$$

By using equations (3.12), (3.17) and (3.18) in (3.7) we obtain

$$-\sum_{i=1}^{E} \tilde{k}_i\dot{\rho}_i^2 - \left(\widetilde{\mathbf{B}}\tilde{\boldsymbol{\mu}}\right)^T \tilde{\mathbf{h}} \leq 0 \tag{3.19}$$

Here we can note clearly that the term $\sum_{i=1}^{E} \tilde{k}_i\dot{\rho}_i^2$ is positive. We have shown that the first term of inequality (3.7) is positive.

Its remains to be shown that the second term of inequality (3.7) is positive. Let us say the second term is positive in the sense that

$$\left(\widetilde{\mathbf{B}}\tilde{\boldsymbol{\mu}}\right)^T \tilde{\mathbf{h}} \geq 0$$

This holds if we assume (3.9) where $\mathbf{E}(\boldsymbol{\rho})$ is positive definite. From the mathematical point of view we have shown that the relation (3.8) together with (3.9) satisfy inequality (3.7). Now we can summarize the model with nutrient flow as consisting of equation (2.35), (3.6),(3.12),(3.9) and (3.11), see [10].

Chapter 4

Implementation

Once all equations are derived for the model, we are interested in how well the model works. In order to perform the calculation we decided to implement the equation in the finite element software TRINITAS (see section Software). Moreover, here we only look at a steady state.

4.1 Steady state model

A steady state model means that all time derivatives are zero. Let us summarize the equations for the steady state model:

$$\widetilde{\mathbf{B}}^T \tilde{\mathbf{h}} = \mathbf{m} \tag{4.1}$$

$$\tilde{\mathbf{h}} = \mathbf{E}(\boldsymbol{\rho})\, \widetilde{\mathbf{B}} \tilde{\boldsymbol{\mu}} \tag{4.2}$$

$$\tilde{\mu}_k = \frac{\partial \psi(\mathbf{c})}{\partial c_k} \tag{4.3}$$

$$0 \in \frac{\partial f_C(\boldsymbol{\rho})}{\partial \rho_i} - \beta \sum_{k=i}^{N} \tilde{\mu}_k \tilde{N}_{ki} a_i + \partial I_{K_i}(\rho_i) \tag{4.4}$$

where

$$\frac{\partial f_C(\boldsymbol{\rho})}{\partial \rho_i} = \mu a_i - e_i(\boldsymbol{\rho}) = \mu a_i - q \rho_i^{q-1} \frac{1}{2} \mathbf{u}^T \tilde{\mathbf{K}}_i \mathbf{u} \tag{4.5}$$

The equation (4.3) becomes

$$\mathbf{c} = \gamma \tilde{\boldsymbol{\mu}} \tag{4.6}$$

By using equation (4.2) and (4.6) in (4.1) we get

$$\frac{1}{\gamma} \widetilde{\mathbf{B}}^T \mathbf{E}(\boldsymbol{\rho})\, \tilde{\mathbf{B}} \mathbf{c} = \mathbf{m} \Leftrightarrow \mathbf{K}_c(\boldsymbol{\rho}) \mathbf{c} = \mathbf{m} \tag{4.7}$$

where $\mathbf{K}_c(\boldsymbol{\rho})$ is a diffusion matrix. By using a fixed point iteration method we calculate

$$\hat{\rho}_i = \left(\frac{e_i(\boldsymbol{\rho}^n) + \beta(\frac{1}{\gamma}) \sum_{k=1}^{N} c_k N_{ki} a_i}{\mu a_i} \right)^{\eta} \rho_i^n \tag{4.8}$$

and then we put $\rho_i^{n+1} = \hat{\rho}_i$ if $\epsilon \leq \rho_i \leq 1$ and otherwise letting ρ_i^{n+1} be ϵ or 1 depending on which inequality is violated. The constant η is a damping factor. When equation (4.8) is converged to one, then the equations of steady state are fulfilled.

This is an optimality criteria like method. The optimality criteria method is a mathematical tool to solve a discreatized structural optimization problem efficiently. Let us also mention that in the classical sizing and topology optimization we calculate the $\boldsymbol{\rho}$ by using the fixed point iteration method like below [19]:

$$\hat{\rho}_i = \left(\frac{e_i(\boldsymbol{\rho}^n)}{\mu a_i} \right)^{\eta} \rho_i^n \tag{4.9}$$

Let us summarize the steps to find $\boldsymbol{\rho}^n$ in the following way

1. Solve $\mathbf{F} = \mathbf{K}(\boldsymbol{\rho}^n)\mathbf{u}$ for $\mathbf{u}$ and calculate $e_i(\boldsymbol{\rho}^n)$
2. Solve $\mathbf{m} = \mathbf{K}_c(\boldsymbol{\rho}^n)\mathbf{c}$ for $\mathbf{m}$.
3. Calculate $\hat{\rho}_i^{n+1} = \left(\frac{e_i(\boldsymbol{\rho}^n) + \beta(\frac{1}{\gamma}) \sum_{k=1}^{N} c_k N_{ki} a_i}{\mu a_i} \right)^{\eta} \rho_i^n$, do a projection onto K_i, set $\boldsymbol{\rho}^n = \boldsymbol{\rho}^{n+1}$ and go to step 1.

4.2 Software

TRINITAS is a finite element software with graphical environment. It was developed by professor Bo Torstenfelt at Linköping University . TRINITAS is used for educational and research purposes. The program is built with FORTRAN and C code. The interface has a menu for geometry modeling, boundary condition definition, mesh generation, simulation and analysing the results. TRINITAS is capable of performing calculations in several areas such as

- Linear static elasticity analysis
- Linear buckling analysis
- Dynamic eigenvalue analysis
- Dynamic modal analysis
- Linear transient direct time integration analysis
- Steady state heat transfer analysis
- transient heat transfer analysis

The TRINITAS software is continuously being developed in many areas such as topology optimization, 3D crack propagation etc [20].

Chapter 5

Solved problems

In this chapter we present two types of test problems; the first test problem we investigate is an MBB beam with special boundary conditions to predict some changes in shape if nutrients inflow is included; for the second test problem we decided to investigate a bone like model to see how the result will be affected if we use the model with inflow of nutrients.

5.1 Test problem one

In order to investigate the theory behind the model, we select an MBB beam with special boundary conditions for the nutrient concentration and inflow of nutrients, see the figure 5.1. The motivation for choosing the model with the boundary conditions presented in the figure 5.1 is partly that we will get an asymmetric solution. If we perform the calculation for the same model without the nutrient concentration and inflow of nutrients, the solution will be symmetric with a symmetry line defined by the force (see the figure 5.2).

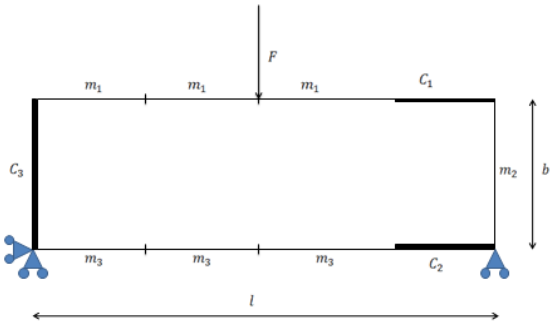

Figure 5.1. MBB beam with a point load (F), nutrient concentration (c) and inflow of nutrients (m).

The dimension of the model and the material properties are presented, see below. The material properties are collected for a bone material.

Dimensions of the model:

- l=1 m
- b=0.3 m
- t=0.3 m

Material properties:

- Elastic modulus: 17E+12 Pa
- κ_0: 0.10E-7

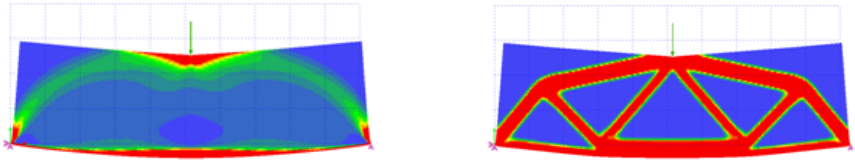

(a) $q = 1$ (b) $q = 3$

Figure 5.2. Classical sizing and topology optimization (by using SIMP formulation)

5.2 Test problem two

Here we decided to investigate a bone-like model to see how the result will be if we use the model with inflow of nutrients. From the reality point of view we select a bone model with boundary condition presented in figure 5.3. The motivation to choose the boundary condition presented in figure 5.3, especially the nutrient concentrations, is that if we make a vertical cut of long bone (see section background) we will get a cross section with space in the middle, which contains nutrients in the form of blood, water etc. The load is not close the reality. In the daily activities several load cases occur. The theory we have derived cannot handle analysis with several load cases, therefore we simply apply the load where it seems to occur mostly.

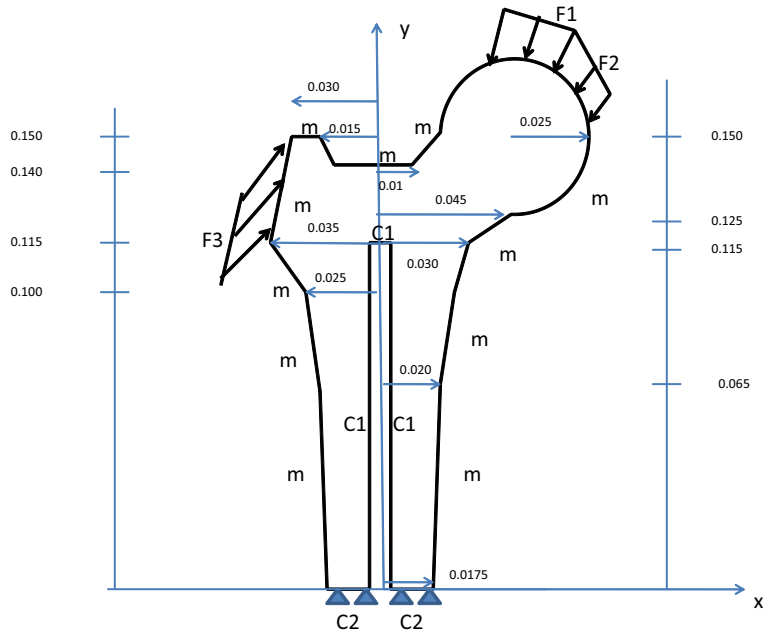

Figure 5.3. bone-like model with load (F), nutrient concentration (c) and inflow of nutrients (m)

The dimensions of the bone model were taken from a skeletal model at Linköping University. The material properties are same as for the MBB beam.

Chapter 6

Results

6.1 Test problem one

In this chapter results will be presented for an MBB beam using various types of analysis, in order to get an understanding of the model. The various types of analysis include how different types of parameters influence the model, such as beta (β), nutrient concentration (c) and mu-value (μ). We will also see how the different loads affect the structure. In addition, we will also see if we get an asymmetric solution. The analysis is done for $q = 1$ and $q = 3$ (see the section topology optimization for more information). It is important to note that the model is not adapted to reality, but should be seen as a test problem.

6.1.1 Analysis for $q = 1$

Analysis with different forces

By performing analysis with different forces we can predict how the structure changes if we have nutrient concentration and inflow of nutrients in the model (see table 6.1). From table 6.1 we can see that only the nutrient concentration in the left hand side is applied, in order to predict a non symmetric solution. Once the model is created in 2D and meshed up to 16384 elements with 4-node quadrilateral elements, the boundary conditions are applied according to table 6.1 and using the settings in TRINITAS as below. The analysis is performed for forces $F = 15000$ N, $F = 20000$ N and $F = 25000$ N, see figure 6.1 with scaling for $F = 15000$ N and figure 6.2 for $F = 20000$ N and $F = 25000$ N. From figure 6.1 and 6.2 we see that when the force increases, the structure becomes thicker. The thickness significantly increases in the surrounding of nutrient concentration in the right hand side of the point load and distributes to the left hand side when the load is increased. We can also note here that the solution obtained is non symmetric. Upper bound and lower bound limits for the design variable ρ, are given below.

Settings in finite element software (TRINITAS):

- Penalty parameter (q): 1
- Damping factor (η): 0.4
- Mu value (μ): 10.9
- Beta value (β) : 0.01
- Upper bound: 3.000
- Lower bound: 0.001

Boundary conditions:

Boundary	Value
m_1	0
m_2	0
m_3	0
c_1	600
c_2	200
c_3	0

Table 6.1. Boundary conditions

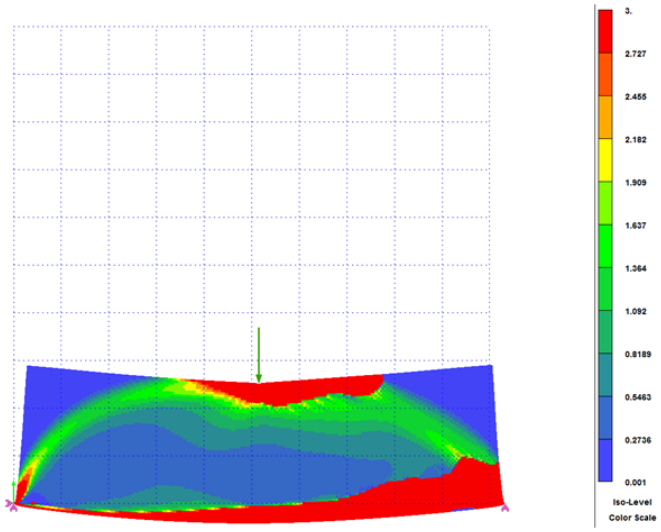

Figure 6.1. $F = 15000$ N with color scale

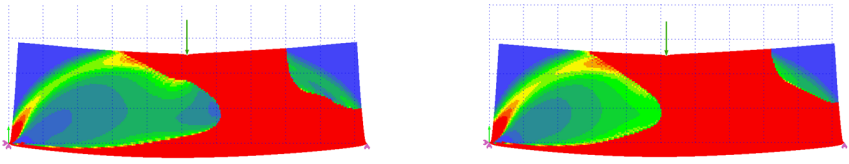

(a) $F = 20000$ N (b) $F = 25000$ N

Figure 6.2. Analysis with different forces for $q = 1$

Analysis with different β values

Beta (β) is a relation between nutrients and material. Here we use the same settings as in the analysis with different forces. The influence of the beta value is simulated by using the same value for point load ($F = 20000$ N) and changing the beta value. The result for beta values 0.02 and 0.03 can be seen in figure 6.3 and the result for 0.01 can be seen in figure 6.2(a). From these figures we can see that when the beta value is increased we get a thicker structure. The structure becomes stiffer when the beta values increase (see table 6.2). The interval for the beta values is estimated to 0.01-5.00. The interval is only valid in the circumstances of the selected model, boundary conditions, settings and applied load.

Displacement (At point load)	$\beta = 0.01$	$\beta = 0.02$	$\beta = 0.03$
Length (m)	0.3466E-04	0.3008E-04	0.2857E-04
X-comp (m)	0.1022E-04	0.9370E-05	0.9292E-05
Y-comp (m)	-0.3312E-04	-0.2859E-04	-0.2701E-04

Table 6.2. Displacement for different values of β ($q = 1$)

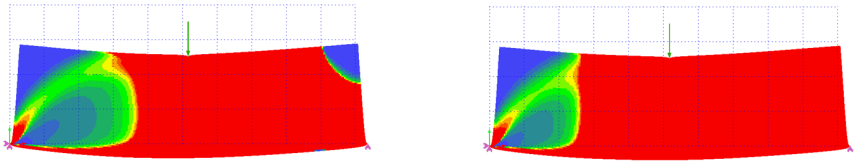

(a) $\beta = 0.02$ (b) $\beta = 0.03$

Figure 6.3. Analysis with different β for $q = 1$

Analysis with different μ values

The influence of μ value is simulated by using the same value for the point load ($F = 20000$ N) and changing the μ value. The result for μ values 6 and 15 can be seen in figure 6.4 and the result for 10.9 can be seen in figure 6.2(a). From these figures we can see that when the μ value is increased we get a thinner structure. The structure becomes stiffer when the μ values decrease (see table 6.3). The interval for the μ values is estimated to 0.01-30. The interval is only valid in the circumstances of the selected model, boundary conditions, settings and applied load.

Displacement (At point load)	$\mu = 6$	$\mu = 10.9$	$\mu = 15$
Length (m)	0.2818E-04	0.3466E-04	0.4654E-04
X-comp (m)	0.9200E-05	0.1022E-04	0.1402E-04
Y-comp (m)	-0.2664E-04	-0.3312E-04	-0.4438E-04

Table 6.3. Displacement for different values of μ ($q = 1$)

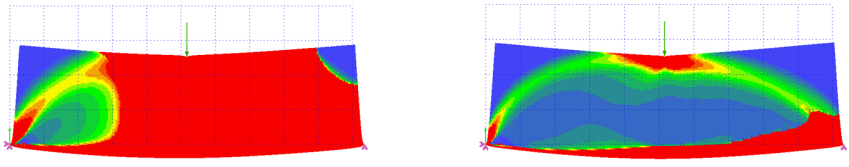

(a) $\mu = 6$ (b) $\mu = 15$

Figure 6.4. Analysis with different μ for $q = 1$

Analysis with different nutrient concentrations

In this part analysis with different nutrient concentrations is performed by changing the value of c_1. The analysis is performed for a constant point load ($F = 20000$ N) and using the same settings as in previous analyses. The result for $c_1 = 800$ and $c_1 = 1000$ can be seen in figure 6.5 and the result for $c_1 = 600$ can be seen in figure 6.2(a). We can see some changes in that there is an elliptic pattern in the boundary at the bottom of the right hand side of the point load. The pattern grows when c_1 increases. The thickness distributes to the left hand side when the concentration, and particularly c_1 increase. We can also see that the structure becomes significantly stiffer when c_1 increases, see table 6.4.

Displacement (At point load)	$c_1 = 600$	$c_1 = 800$	$c_1 = 1000$
Length (m)	0.3281E-04	0.3125E-04	0.3055E-04
X-comp (m)	0.1084E-04	0.1046E-04	0.1012E-04
Y-comp (m)	-0.3097E-04	-0.2945E-04	-0.2882E-04

Table 6.4. Displacement for different values of c_1

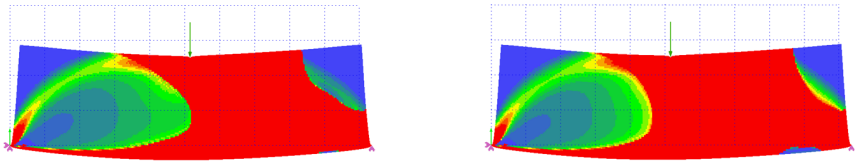

(a) c_1=800 (b) c_1=1000

Figure 6.5. Analysis with different nutrient concentrations

6.1.2 Analysis for $q = 3$

The methodology for analyzing $q = 3$ is the same as for $q = 1$, but with different settings.

Analysis with different forces

In order to see how the structure changes its shape if $q = 3$ is used, we decided to use the same boundary conditions as for the first model analyzed with $q = 1$ and settings as below. The analysis is performed for point loads $F = 30000$ N, $F = 33000$ N and $F = 35000$ N, see figure 6.6. From figure 6.6 we can see significant changes of thickness in the beam bars and some changes in location for the beam bars. We can also note the non symmetrical solution for $q = 3$ like we did for $q = 1$. In order to prevent checkerboard pattern results a filter radius is used see [19].

Settings in finite element software (TRINITAS):

- Penalty parameter (q): 3
- Damping factor (η): 0.5
- Mu value (μ): 50
- Beta value (β): 0.55E-06
- Filter radius: 0.014
- Upper bound: 3.000
- Lower bound: 0.001

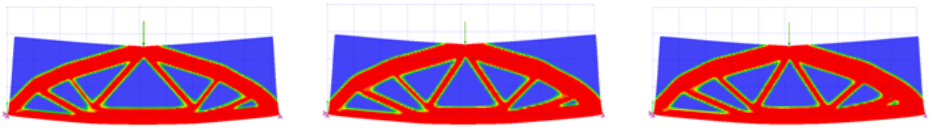

(a) $F = 30000$ N (b) $F = 33000$ N (c) $F = 35000$ N

Figure 6.6. Analysis with different forces for $q = 3$

Analysis with different β values

Here we use the same settings as for the analysis with different forces. The influence of the beta value is simulated by using the same model as for point load $F = 30000$ N and changing the beta value. The result for beta values 0.25E-06 and 0.40E-06 can be seen in figure 6.7 and the result for 0.55E-06 can be seen in figure 6.6(a). From these figures we can see that when the beta value is increased we get thicker beam bars and changes in the size of spaces between bars. That can especially be noted in the right hand side of the point load. The structure becomes stiffer when the beta value increases, see table 6.5.

Displacement (At point load)	β = 0.25E-06	β = 0.40E-06	β = 0.55E-04
Length (m)	0.6609E-04	0.6713E-04	0.6577E-04
X-comp (m)	0.2004E-04	0.2027E-04	0.2024E-04
Y-comp (m)	-0.6298E-04	-0.6400E-04	-0.6258E-04

Table 6.5. Displacement for different values of β ($q = 3$)

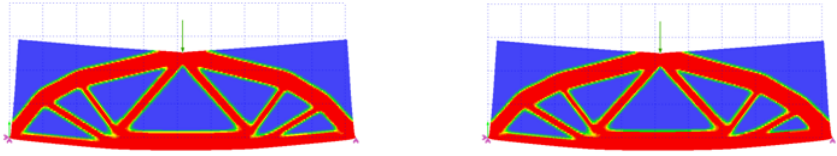

(a) β=0.25E-06 (b) β=0.40E-06

Figure 6.7. Analysis with different β values for $q = 3$

Analysis with different μ values

The influence of μ value is simulated by using the same model as for β=0.25E-06, with point load $F = 30000$ N and changing the μ value. The result for μ values 25 and 75 can be seen in figure 6.8 and the result for 50 can be seen in figure 6.7(a). From these figures we can see that when the μ value is increased we get thinner beam bars. The structure becomes stiffer when the μ values decrease. We can also note here that for small values of μ we get a non symmetric solution, but for larger μ values we get a symmetric solution and close to classical topology optimization with SIMP formulation, as shown in figure 5.2. This is also notable in analysis for $q = 1$ with different μ values.

Displacement (At point load)	$\mu = 25$	$\mu = 50$	$\mu = 75$
Length (m)	0.5312E-04	0.6609E-04	0.8062E-04
X-comp (m)	0.1650E-04	0.2004E-04	0.2412E-04
Y-comp (m)	-0.5049E-04	-0.6298E-04	-0.7692E-04

Table 6.6. Displacement for different values of μ ($q = 3$)

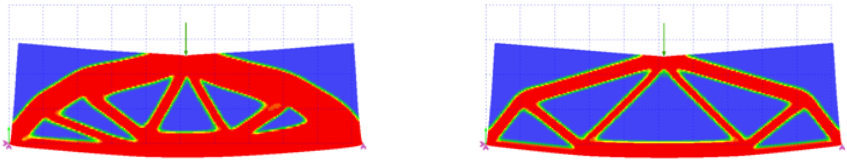

(a) μ=75 (b) μ=25

Figure 6.8. Analysis with different μ values for $q = 3$

6.2 Test problem two

For test problem two the analysis is not done in the same range as in the previous model (a MBB beam). The results from the analysis are uncertain due to the complex geometry, which makes the mesh generation irregular. The test problem is only analyzed to see how the bone-like model will act if topology optimization with nutrients inflow is used. Once the model is created in 2D according to figure 5.3 and meshed up to 3760 elements with 4-node quadrilateral elements, the boundary conditions are applied according to table 6.7 and using settings in TRINITAS as below. First the analysis is performed for the classical sizing optimization ($q = 1$) (see figure 6.9) and the classical topology optimization ($q = 3$) (see figure 6.10).

Settings in finite element software (TRINITAS):

- Penalty parameter (q): 1 and 3
- Damping factor (η): 0.4 (for the $q = 1$ and $q = 3$)
- Upper bound: 3.000
- Lower bound: 0.001

Boundary conditions:

Boundary	Value
F_1	x=-400 N, y=-1500 N
F_2	x=-200 N, y=-1000 N
F_3	x=300 N, y=900 N

Table 6.7. Boundary condition (without nutrients)

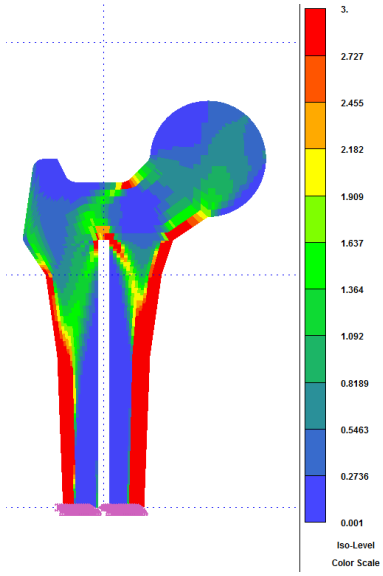

Figure 6.9. The classical sizing optimization ($q = 1$)

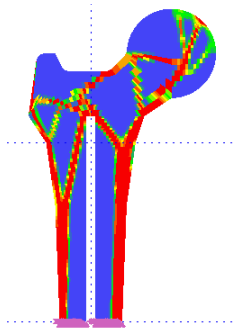

Figure 6.10. The classical topology optimization ($q = 3$)

Analyzing in the same way as for the classical sizing optimization ($q = 1$) we include nutrients inflow by using boundary condition presented in table 6.8 and using the settings as below in TRINITAS. In figure 6.11 we can see the result for sizing optimization with inflow of nutrients and we can also note that the model (bone) becomes thicker compared to the classical sizing optimization.

Settings in finite element software (TRINITAS):

- Penalty parameter (q): 1
- Damping factor (η): 0.4

- Mu value (μ): 1.05
- Beta value (β) : 0.00038
- Upper bound: 3.000
- Lower bound: 0.001

Boundary conditions:

Boundary	Value
F_1	x=-400 N, y=-1500 N
F_2	x=-200 N, y=-1000 N
F_3	x=300 N, y=900 N
c_1	500
c_2	100
m	0

Table 6.8. Boundary condition (including nutrients inflow)

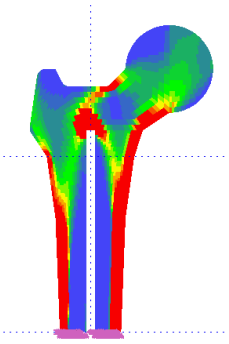

Figure 6.11. Analysis with inflow of nutrients ($q = 1$)

Analyzing in the same way as for the classical topology optimization ($q = 3$) we include nutrients inflow by using boundary condition presented in table 6.8 and using the following settings as below in TRINITAS. In figure 6.12 we can see the result for topology optimization with inflow of nutrients and we can also note that the model (bone) becomes thicker where the load is applied.

Settings in finite element software (TRINITAS):

- Penalty parameter (q): 3
- Damping factor (η): 0.4
- Mu value (μ): 3.93534
- Beta value (β) : 0.00015
- Filter radius: 0.0022
- Upper bound: 3.000
- Lower bound: 0.001

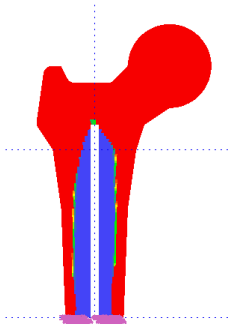

Figure 6.12. Analysis with inflow of nutrients ($q = 3$)

Chapter 7

Discussion of results

In test problem one, we investigated an MBB beam by using various types of analysis, in order to get an understanding of how well the model works. The various types of analysis include how different types of parameters influence the model, such as beta (β), nutrient concentration (c) and mu-value (μ). In addition, we look at how the structure is affected if we use different loads. In test problem two; we investigate a bone-like model to see how the result will be if we use topology optimization with nutrients inflow. Let us first discuss the result achieved for test problem one.

For the analysis with different loads we have observed that the structure becomes thicker were the load is applied. In section background we mention Wolff's law, according to which the bone grows and remodels in response to applied load. If we compare Wolff's law and the result achieved for different loads this gives us some confidence in the applicability of the model. Biological structures like bone do not grow and remodel only in response to the applied load, but are also subject to other process that build up the structures. Parameters like beta (β) and nutrient concentration (c) play an important role in nutrients transport and building of the structure. The result for larger values of β and nutrient concentration (c) gives a thicker structure in the entire domain (see section result). We also made an assumption of Fick's law of diffusion. Fick's law of diffusion describes the flux from high concentration to low concentration. This phenomenon is observed in analysis with different nutrients concentration (c); we can see that the structure tends to be built up where the concentration is high and continues to be built in the direction from high concentration to low concentration. In analysis with mu-value (μ), which represents cost of material the result gives a thinner structure if we have larger value of μ. It is also notable that for the larger value of μ the second term of the equation is neglected so we get a result close to the classical optimization (see the section result).

Concerning test problem two, the results from the analysis are uncertain due to the complex geometry, which makes the mesh generation irregular, but we get a good result that mirrors the analysis we have done in test problem one.

In this project we only look at a steady state model. In the future it would be

very interesting to investigate a model with time dependency (transient analysis) so we can see the problem as an evolution problem with different load cases. Especially for a structure like bone, where different load cases occur in daily activities. In this area TRINITAS is continuously being developed to handle problems like this.

Appendix A

Convex analysis

Let $f : R^n \to R \cup \{\infty\}$ be a real-valued convex function. A subgradient $y \in R^n$ of f at x is defined by

$$f(z) - f(x) \geq y^t(z - x) \quad \forall z \in R^n$$

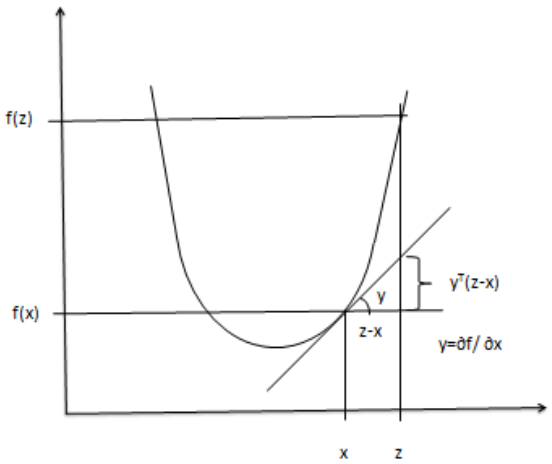

Figure A.1. An illustration

The relation above is illustrated in figure A.1. The set of all subgradients at x, see figure A.2, is the subdifferential, that is denoted as below:

$$y \in \partial f(x)$$

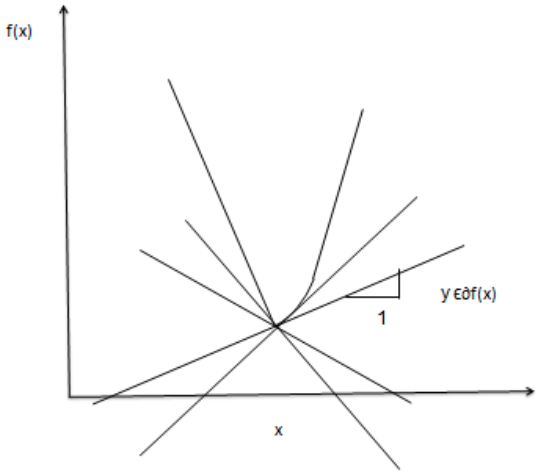

Figure A.2. The set of all subgradients at x

Let C be a convex set given by

$$C = \{x \in R^n | f(x) \leq 0\}$$

The indicator function of a convex set C is defined as

$$I_C(x) = \begin{cases} 0 & \text{if } x \in C \\ \infty & \text{if } x \notin C \end{cases}$$

Consider the multi-valued relation

$$y \in \partial I_C(x)$$

The relation above can be written like

$$y = \lambda \frac{\partial f}{\partial x}$$

$$f \leq 0,\ \lambda \geq 0,\ f\lambda = 0$$

This is called the Karush-Kuhn-Tucker (KKT) conditions [11].

Bibliography

[1] Bartel, Donald L. Davy, Dwight T. Keaveny, Tony M. Orthopaedic biomechanics: mechanics and design in musculoskeletal systems. Pearson Prentice Hall bioengineering, 2006.

[2] A. Klarbring, B. Torstenfelt. Dynamical Systems and Topology Optimization, *Structural and Multidiciplinary Optimization* 42:179-192, 2010.

[3] T.P. Harrigan, J.J. Hamilton. Optimality conditions for finite element simulation of adaptive bone remodeling, *International Journal of Solids and Structures* 29(23):2897-2906, 1992.

[4] T.P Harrigan, J.J. Hamilton. Necessary and sufficient conditions for global stability and uniqueness in finite element simulations of adaptive bone remodeling, *International Journal of Solids and Structures* 31(1):97-107, 1994.

[5] T.P. Harrigan, J.J. Hamilton. Bone remodeling and structural optimization, *Journal of Biomechanics* 27(3):323-328, 1994.

[6] J.D. Humphrey, S.L Delange. An Introduction to Biomechanics Solids and Fluids, Analysis and Design, Springer, 2004.

[7] S.C. Cowin, S.B Doty. Tissue Mechanics, Springer, 2007.

[8] S.C. Cowin. Bone Mechanics Handbook. Second Edition, CRC PRESS, 2001.

[9] M.P. Bendøse, O. Sigmund. Topology Optimization: theory, methods and applications, Springer, 2003.

[10] A. Klarbring. Topology Optimization, Dynamical Systems, Thermodynamics and Growth, Submitted.

[11] N. Strömberg. On the Thermodynamics of Non-Smooth Phenomena, Paper 2.

[12] A. Klarbring. Unified evolutionary view on bone remodeling and topology optimization, Submitted.

[13] R.M. Berne, M.N. Levy, B.M Koeppen, B.A Stanton. Physiology. Fifth Edition, Mosby, 2000.

[14] A. Persson, L.C. Böiers. Analys i flera variabler, Studentlitteratur, 2005.

[15] A. Klarbring. Models of Mechanics, Springer, 2006.

[16] B. Torstenfelt. Finite Elements *"from the early beginning to the very end"*: An Introduction to Elasticity and Heat Transfer Applications, *Preliminary Edition* LiU-IEI-s–08/535–SE.

[17] N. Ottensen, H. Petersson. Introduction to the finite element method, Prentice hall, 1992.

[18] R.D. Cook, D.S. Malkus, M.E. Plesha, R.J. Witt. Concepts and applications of finite element analysis. Fourth Edition, WILEY, 2002.

[19] P.W. Christensen, A. Klarbring An Introduction to Structural Optimization, Springer, 2009.

[20] B. Torstenfelt. TRINITAS, a Finite Element stand-alone tool for Conceptual design, Optimization and General finite element analysis, Introductional Manual